Frontiers of Information Technology & Electronic Engineering
www.jzus.zju.edu.cn; engineering.cae.cn; www.springerlink.com
ISSN 2095-9184 (print); ISSN 2095-9230 (online)
E-mail: jzus@zju.edu.cn

Target detection for multi-UAVs via digital pheromones and navigation algorithm in unknown environments*

Yan SHAO[1], Zhi-feng ZHAO‡[1,2], Rong-peng LI[1], Yu-geng ZHOU[3]

[1]*College of Information Science and Electronic Engineering, Zhejiang University, Hangzhou 310027, China*

[2]*Zhejiang Lab, Hangzhou 311121, China*

[3]*Institute of Wanfeng Jinyuan Holding Group Co., Ltd., Shaoxing 312000, China*

E-mail: shaoy@zju.edu.cn; zhaozf@zhejianglab.com; lirongpeng@zju.edu.cn; yugeng.zhou@wfjyjt.com

Received Nov. 30, 2019; Revision accepted Mar. 8, 2020; Crosschecked Mar. 31, 2020

Abstract: Coordinating multiple unmanned aerial vehicles (multi-UAVs) is a challenging technique in highly dynamic and sophisticated environments. Based on digital pheromones as well as current mainstream unmanned system controlling algorithms, we propose a strategy for multi-UAVs to acquire targets with limited prior knowledge. In particular, we put forward a more reasonable and effective pheromone update mechanism, by improving digital pheromone fusion algorithms for different semantic pheromones and planning individuals' probabilistic behavioral decision-making schemes. Also, inspired by the flocking model in nature, considering the limitations of some individuals in perception and communication, we design a navigation algorithm model on top of Olfati-Saber's algorithm for flocking control, by further replacing the pheromone scalar to a vector. Simulation results show that the proposed algorithm can yield superior performance in terms of coverage, detection and revisit efficiency, and the capability of obstacle avoidance.

Key words: Collective intelligence; Digital pheromones; Artificial potential field; Navigation algorithm
https://doi.org/10.1631/FITEE.1900659 **CLC number:** TP11

1 Introduction

The concept of collective intelligence (or swarm intelligence) was proposed in the 1980s and is currently receiving more attention. By studying the cluster activities in nature, collective intelligence explores methods to solve complex problems with decentralized control and limited prior knowledge. The primary advantage of this technology lies in its scalability, flexibility, and robustness (Senanayake et al., 2016). It is becoming a consensus that collective intelligence emerges in the process of continuous evolution through a simple multi-agent system, which is represented mainly by the ant colony optimization (ACO) algorithm, the flocking algorithm, and particle swarm optimization (PSO); the major difference between PSO and the previous two algorithms lies in that particles replace individual members in the population.

On the other hand, with the continuous innovation of the unmanned aerial vehicle (UAV) technology, more and more missions prefer using multi-UAVs to carry out reconnaissance in some extreme conditions such as border and harbor patrol, landmine detection, search, and rescue (Alfeo et al., 2018a). Thus, collective intelligence has become fashionable for performing tasks such as obstacle

‡ Corresponding author

* Project supported by the National Key R&D Program of China (No. 2017YFB1301003), the National Natural Science Foundation of China (Nos. 61701439 and 61731002), the Zhejiang Key Research and Development Plan (Nos. 2019C01002 and 2019C03131), the Project sponsored by Zhejiang Lab (No. 2019LC0AB01), and the Zhejiang Provincial Natural Science Foundation of China (No. LY20F010016)

ORCID: Yan SHAO, https://orcid.org/0000-0003-2522-4951; Zhi-feng ZHAO, https://orcid.org/0000-0002-5479-7890

avoidance, target seeking, and goal attacking in a multi-UAV system (van Dyke Parunak et al., 2002). It has also been applied in domains like traffic control (Ando et al., 2006) and urban hotspot detection (Alfeo et al., 2018b).

One of the most important ingredients in collective intelligence is pheromone or stigmergy. Some insects in a cluster communicate and collaborate by producing and sensing chemicals called pheromones in a shared environment. This is an indirect communication mechanism known as stigmergy. Digital pheromones involve the aforementioned mechanism to multi-UAV system control, so as to enable agents to make decisions. Digital pheromones are one of the significant domains of stigmergic mechanism, and they have some attractive features like simplicity, scalability, and robustness (Sauter et al., 2005). In complex multi-agent systems, rather than complex computation, direct communication, and centralized control, agents can instead perform macro-ordered behaviors through indirect communications via stigmergy.

In this study, we use digital pheromones with different semantics and concentrations to highlight different targets, obstacles, and routes. In particular, we combine three characteristics of digital pheromones to form artificial pheromone potential fields. Within the field of stigmergy, some fundamental hardware support technologies are essential. For example, the place saving the local pheromones is called the place agent, which can be implemented by radio frequency identification (RFID) (Tang et al., 2019) or unattended ground sensors (UGSs) networked through wireless communication (Sauter et al., 2005) or other distributed memories. Synthesizing artificial pheromone potential fields from all place agents can form a global pheromone map, which contains all information about the current environment and needs to be updated in each iteration. The three characteristics are as follows (Sauter et al., 2005):

1. Aggregation (realizing the fusion of information)

Individuals can deposit and withdraw digital pheromones with different semantics in the shared environment. Place agents need to integrate the pheromones with the same semantics, and save and update the current map.

2. Evaporation (truth maintenance)

Pheromones need to be evaporated over time to ensure that old, outdated information has been processed.

3. Diffusion (information diffusion and dissemination)

The spread of digital pheromones to neighboring areas leads to the formation of pheromone gradients. Pheromone gradients can further guide an individual's trajectory.

Another key point is the flocking algorithm. Flocking behavior exists in the form of a flock of birds, school of fish, swarm of bacteria, and so on in nature (Su et al., 2009). Reynolds (1987) introduced three heuristic rules that lead to creation of the first computer animation of flocking. They are known as cohesion, separation, and alignment rules. Under the assumptions of Reynolds (1987), Olfati-Saber (2006) proposed a flocking algorithm. The main idea is that incorporating a navigational feedback enables a group of agents to track a virtual leader. Instead of using a virtual leader, we use a leader UAV who leads other (limited) drones in reaching the target zone through sensing digital pheromones.

In this study, we introduce collective intelligence and design three types of digital pheromones with different semantics, so as to instruct multi-UAV systems for target detection and revisit in environments with limited prior knowledge. For a single UAV, it just needs to communicate with the nearest place agent to obtain the local information and make decisions. Therefore, each UAV can make moving decisions. It achieves distributed control and avoids communication delay and congestion due to centralized control or direct communication between every two agents in the system. We also integrate the digital pheromone mechanism with Olfati-Saber's flocking algorithm to design a navigation algorithm considering the limitations of some UAVs in perception and communication.

2 Related work

The flexible, unmanned, and high cost-benefit features of a multi-UAV system make it widely suited for searching and tracking algorithms. Senanayake et al. (2016) presented several control algorithms derived from collective intelligence, such as PSO (Eberhart and Kennedy, 1995; Kennedy and Eberhart, 1995), artificial bee colony (ABC) optimization

(Karaboga, 2005), and ACO (Dorigo et al., 1999).

On this basis, researchers proposed many innovative algorithms to adapt to the requirements in different scenarios. van Dyke Parunak et al. (2002) pointed out an algorithm instructing potential field via pheromones and applied this mechanism to the problem of controlling air combat missions. Kuyucu et al. (2015) presented a guided probabilistic exploration via combining random movement with pheromone-based stigmergic guidance. They observed a super-additive effect of adding new robots to exploration due to the reduction in the number of areas to be explored and the number of revisits that each robot has to do while crossing already explored areas. This provides a higher efficiency than linear increase. Micieta et al. (2018) defined a technological framework, coordination and control of decentralized systems architecture (CODESA), to coordinate and control decentralized systems, and also defined the data structures of selected pheromone types, which help the decentralized systems work more efficiently in a pheromone container. Liu et al. (2018) designed a cognitive map, consisting of the target probability map, the uncertain map, and the digital pheromone map, to reduce the uncertainty of the search area as soon as possible. Alfeo et al. (2018a) aimed to combine three biologically inspired processes, stigmergy, flocking, and evolution, to improve the efficiency of target search. Differential evolution, one of the most powerful stochastic real-parameter optimization algorithms, has been used mainly to tune appropriate structural parameters for a certain scenario. The target identification error caused by imperfect sensors has also been considered in Alfeo et al. (2018c). Dai et al. (2020) proposed a collective intelligence evaluation framework to define and quantify the intelligence level of a heterogeneous agent group; using the improved anytime universal intelligence test (AUIT), the existing evaluation of a homogeneous agent group can be extended to the above-mentioned heterogeneous agent group.

Flocking algorithms for multi-agent dynamic systems have also received a lot of attention. Soria et al. (2019) studied the performance difference of Reynolds's flocking algorithm between simulations and reality when reducing the view and the orientation of the visual sensors. Vásárhelyi et al. (2018) proposed a flocking construction for real drones incorporating an evolutionary optimization framework with carefully chosen order parameters and fitness functions. They tested their construction on real hardware and finished the largest aerial distributed outdoor system.

Based on the above algorithms, we focus on the artificial pheromone potential field formed by pheromones. This field is used to guide individual decision-making and ameliorate the flocking algorithm in solving the limitations of some individuals. We have paid more attention to the decision-making scheme via involving vector pheromones (Tang et al., 2019) while many previous studies preferred using scalar pheromones. Considering that real scenarios have many different components rather than targets only, we classify three types of digital pheromones, propose the updating strategies for each semantic pheromone, and optimize the fusion algorithm for them.

3 Scenario design

We envision that our proposed algorithm can be applied to significant scenarios. All of these conditions have one thing in common that the multi-UAV system knows the approximate position of the target region like rescue of survivors after a disaster, exploration of geological resource, and detection of the leaking oil barrels in the ocean. Individuals need to arrive at the general region based on the aforementioned limited knowledge. After that, they carry out target detection and revisit without prior knowledge in the specific regions. Therefore, we design the scenarios as follows:

We assume that the whole task space is a two-dimensional (2D) $P \times Q$ lattice map with boundaries (walls), some obstacles, and one target region (Fig. 1). Leaders, having comparative advantages in perception and communication, need to guide others to the target region and carry out the detecting and revisiting work.

As depicted in Fig. 2, after further partitioning the target region into $M \times N$ spots, there are several randomly distributed targets and some obstacle areas. The system requires each agent make independent decisions to find the targets while avoiding obstacles. Afterwards, targets need to be revisited again after a fixed period T. As for UAVs, we refer to the UAV movement model in Yang et al. (2017), which defines that UAVs move only between the

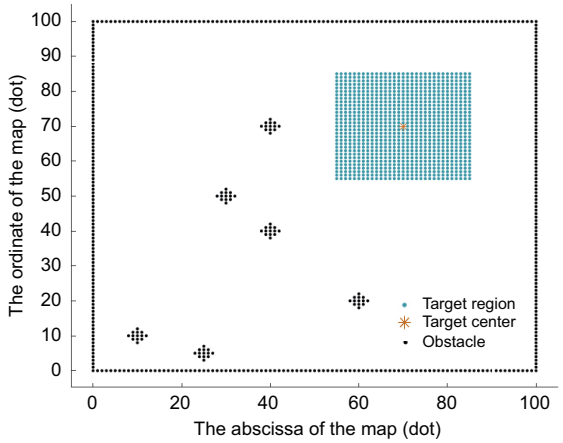

Fig. 1 Scenario model of the navigation algorithm (100 × 100). The scenario model of the whole task space is $P \times Q$

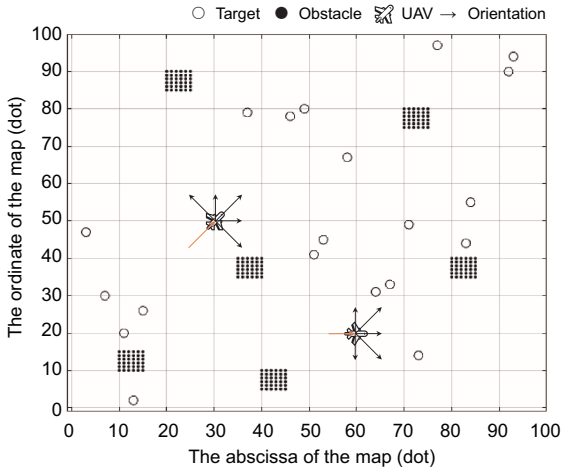

Fig. 2 Scenario model (100 × 100) of the target region $M \times N$ (a UAV has five orientations with different costs to select in each iteration)

adjacent points for five orientations. Different costs should be paid for various orientations.

4 Target detection and revisit via digital pheromones

In this section, we first solve the problem of target detection and revisit in the target region. When detecting targets in an unknown environment, initial path planning and artificial obstacle avoidance may be necessary for each agent. We introduce the ACO algorithm combined with stigmergy via digital pheromones to detect and revisit the targets. There is no need for default routes and involving artificial adjustments. The system can grasp the dynamics of the target region automatically.

4.1 Digital pheromone update

Depending on the situation with multiple components, three kinds of semantic digital pheromones are involved to mark targets, obstacles, and the routes of UAVs, respectively. Given these characteristics of digital pheromones, we design diverse update functions for these digital pheromones based on the traditional digital pheromone function.

1. Target pheromones

The update of target pheromones (Liu et al., 2018) at the i^{th} point in the t^{th} step, $\tau(i,t)$, is implemented by

$$\begin{aligned}\tau(i,t) =&(1-E_\tau)\big\{(1-G_\tau)[\tau(i,t-1)\\&+k_\tau(i,t)\cdot d_\tau]+g_\tau(i,t)\big\},\end{aligned} \tag{1}$$

where $E_\tau \in [0,1)$ represents the evaporation coefficient of target pheromones, $G_\tau \in [0,1)$ means the diffusion coefficient, and $k_\tau(i,t) \in \{0,1\}$ is a binary switch devoted to achieve the revisit algorithm. $k_\tau(i,t)=1$ declares that this point has a target which has been found and needs to be revisited. Otherwise, it means that there is no target or the target in this point has no need to be revisited. Hence, the switch is closed, $k_\tau(i,t)=0$. d_τ is the pheromone concentration produced by targets in one iteration. The accumulated concentration diffusing from neighborhood is $g_\tau(i,t)$, which is calculated by

$$g_\tau(i,t)=\sum_{j\in N(i)}\frac{G_\tau}{|N(j)|}\Big[\tau(j,t-1)+k_\tau(j,t)\cdot d_\tau\Big], \tag{2}$$

where $N(i)$ identifies the adjacent point set for the i^{th} point, and $|N(i)|$ is the number of these points. We sum over the variations whose indices are in $N(i)$.

2. Obstacle pheromones

As for obstacle pheromones at the i^{th} point in the t^{th} step, similar to target pheromones, the update functions are displayed as follows:

$$\begin{aligned}\varepsilon(i,t)=&(1-E_\varepsilon)\{(1-G_\varepsilon)[\varepsilon(i,t-1)\\&+k_\varepsilon(i,t)\cdot d_\varepsilon]+g_\varepsilon(i,t)\},\end{aligned} \tag{3}$$

$$g_\varepsilon(i,t)=\sum_{j\in N(i)}\frac{G_\varepsilon}{|N(j)|}\Big[\varepsilon(j,t-1)+k_\varepsilon(j,t)\cdot d_\varepsilon\Big], \tag{4}$$

where the meanings of E_ε, G_ε, k_ε, and $g_\varepsilon(i,t)$ are similar to those for the target pheromones.

3. Path pheromones

When a multi-UAV system begins searching in an unknown area, due to the fact that there is no prior knowledge, a random search seems to result in a high repetition rate. The purpose of path pheromones is to mark the path passed recently. This mechanism prevents the repeated visit in a short time, thus being capable of reducing the difficulty in searching and increasing the global coverage rate compared to an exhaustive search algorithm. The update strategy of path pheromones (Yang et al., 2017) at the i^{th} point in the $(t+1)^{\text{th}}$ step is shown as follows:

In the initialization phase, we set the path pheromones for each point on the map to σ_0. After completing path selection and movement, the path pheromones at the individual's current location will decrease:

$$\sigma(i,t+1)=\sigma(i,t)-\Delta\sigma(i,t). \tag{5}$$

The pheromones of the next step are under the influence of all agents in the system. The following function accounts for how the decrease is calculated:

$$\Delta\sigma(i,t)=\sum_{k=1}^{m}\Delta\sigma_{ij}^{k}(t), \tag{6}$$

where k is the identification of each individual, m is the amount, and $\Delta\sigma_{ij}^{k}(t)$ represents the effect of the k^{th} UAV at the j^{th} point on the path pheromones at the i^{th} dot:

$$\Delta\sigma_{ij}^{k}(t)=\begin{cases}\dfrac{1}{2\sqrt{2\pi}}\exp\left(-\dfrac{(Q/D_{ij})^2}{2}\right)\cdot\sigma_0, & \\ & D_{ij}\le D_0,\\ 0.9\sigma_0, & D_{ij}=0,\\ 0, & D_{ij}>D_0.\end{cases} \tag{7}$$

The distance from the i^{th} dot to the j^{th} dot is D_{ij}. D_0 identifies the individual's range of influence. Q represents the attenuation coefficient of pheromones. As for the coefficient 0.9, it represents the pheromone decay rate of the current point, which should decay much faster than neighbors, since it is the point that has been detected and needs no review recently. Finally, to prevent negative values and excessive fluctuation of path pheromones, we constrain the values in $[\sigma_{\min},\sigma_0]$.

$$\sigma(i,t+1)=\begin{cases}\sigma_{\min}, & \sigma<\sigma_{\min},\\ \sigma_0, & \sigma>\sigma_0,\\ \sigma(i,t+1), & \text{otherwise.}\end{cases} \tag{8}$$

4.2 Decision-making scheme

In addition to the map update strategy, an appropriate moving decision-making scheme is crucial. Each UAV respectively communicates with the nearby place agent to obtain the local pheromone map and integrate the information. Based on the probabilistic function, it can choose a proper direction along which to move. Yang et al. (2017) proposed to take eight adjacent points as a reference. To obtain more information and take account of practical constraints, the sensor range has to be considered. As shown in Fig. 3, we consider only the influence of points within the sensor range.

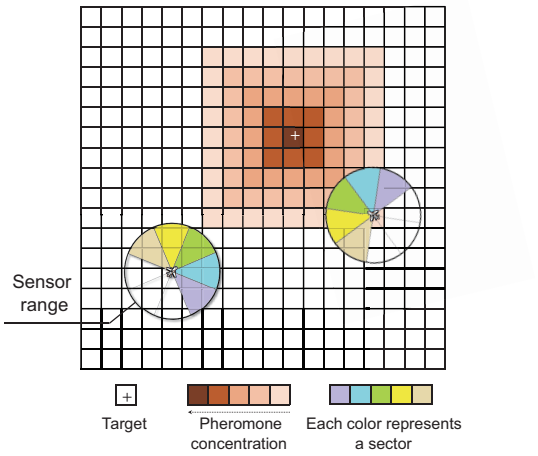

Fig. 3 Sensor range and sector division of UAVs. Different color sectors represent five different orientations and the orange block means different concentration of pheromones. The darker the color, the higher the concentration. References to color refer to the online version of this figure

For simplicity of calculation, we divide the forward direction into five sectors based on UAV movement constraints and accumulate the pheromones in each sector. The mean values of the target pheromones, obstacle pheromones, and path pheromones in the j^{th} direction are expressed by τ_j, ε_j, and σ_j, respectively.

After considering different semantic digital pheromone concentration in different orientations and the costs for angle conversion and distance movement, Eq. (9) is used for individual decision-making. This takes all above factors into account. UAVs need to select one direction with the highest probability

and move on.

$$P_{ij}^{k}=\frac{(\lambda_{\mathrm{Ta}}\tau_j+\lambda_{\mathrm{Th}}\varepsilon_j+\lambda_{\mathrm{Tr}}\sigma_j)^{\alpha}\eta_{ijk}^{\beta}}{\sum_{j\in J_i^k}(\lambda_{\mathrm{Ta}}\tau_j+\lambda_{\mathrm{Th}}\varepsilon_j+\lambda_{\mathrm{Tr}}\sigma_j)^{\alpha}\eta_{ijk}^{\beta}},\quad(9)$$

where $j\in J_i^k$ and P_{ij}^k is the probability that the k^{th} UAV at the i^{th} point chooses to move to the j^{th} point. $\lambda_{\mathrm{Ta}}\in[0,1]$, $\lambda_{\mathrm{Th}}\in[-1,0]$, and $\lambda_{\mathrm{Tr}}\in[0,1]$ represent the relative weights of impact of target, obstacle, and path pheromones on the direction selection decision, respectively. Notably, since the obstacle item is a negative item, the weight λ_{Th} should be negative. Besides, the sum of the weights should be 1. J_i^k is the set of points which are accessible. We sum over the variations whose indices are in J_i^k. α and β are used to find the balance between digital pheromones and physical costs η_{ijk}, defined as

$$\eta_{ijk}=\begin{cases}\dfrac{1}{4}\eta_{ij}, & \theta=0^{\circ},\\ \dfrac{5}{24}\eta_{ij}, & \theta=45^{\circ},\\ \dfrac{1}{6}\eta_{ij}, & \theta=90^{\circ},\\ 0, & \text{otherwise},\end{cases}\quad(10)$$

where θ means the angle of orientation changed in one iteration. The costs of different degrees are different in terms of diverse coefficients:

$$\eta_{ij}=\begin{cases}1.4, & D_{ij}=1,\\ 1, & D_{ij}=\sqrt{2},\\ 0, & \text{otherwise}.\end{cases}\quad(11)$$

Furthermore, on the basis of a genetic algorithm, UAVs are divided into random subgroups and information subgroups randomly in each step. The random subgroup considers only the physical costs, while the information subgroup makes decisions according to all factors. This mechanism can reduce resource wastage and avoid local optima because one target may appeal to more than one agent while some targets are not found all the time. The key algorithm is summarized as Algorithm 1.

4.3 Simulation and results

To fully verify the robustness and adaptability of the algorithm, various maps with different sizes and numbers of targets are tried. In this subsection, 50×50 and 100×100 lattice maps are chosen typically. Important parameters are given in Table 1.

Algorithm 1 Target detection and revisit

Input: the map of targets, obstacles, and multi-UAV distribution
Output: the path map of UAVs

```
for step ← 1 to N_c do
  for k ← 1 to N_UAV do
    if having targets in the sensor range then
      Go there, mark them, and turn on the timer
    end if
    if having obstacles in the sensor range then
      Mark them
      Turn on the obstacle switch k_ε(i,t) = 1
    end if
    Calculate the probability of each direction
    Select the maximum and move on
  end for
  Map update
end for
return
```

We analyze the simulation results from the following four aspects.

4.3.1 Target acquisition rate

The target acquisition rate demonstrates mainly the system's efficiency of target detection guided by an artificial pheromone potential field. Fig. 4 shows the results of average target acquisition rates after averaging 10 simulations in two maps of different sizes. Remarkably, in Fig. 4, the number of iterations increases linearly with the number of targets acquired in the early stage. Later, finding a new target requires more iterations and is probably the cause for more obstacles needing to be avoided and more targets needing to be revisited.

4.3.2 Revisit response rate

Once the target is acquired, it still needs to be accessed again for a fixed period T to monitor its dynamics. Fig. 5 expresses the number of response iterations required by the process whereby the multi-UAV system reaches the target point again after it sends revisiting signals by generating target pheromones. In this part, the operation of averaging from multiple tests is also involved. In the 50×50 map, the number of iterations required for revisiting is basically controlled within 20 to 80. Although the value of the third test may be slightly larger, the average value is mainly in line with our expectation. As for the 100×100 case, the first few revisits cost

Table 1 Simulation parameters of the target detection and revisit algorithm

Parameter	Description	Value(s)
$M \times N$	Map size	50×50, 100×100
TarN	Number of targets	5, 20
T	Revisit period	500, 800
N_c	Number of total iteration steps	3000, 10 000
SD	Sensor radius	4, 4
E_τ	Evaporation coefficient of target pheromones	0.2
G_τ	Diffusion coefficient of target pheromones	0.2
d_τ	Pheromone concentration produced by targets in one iteration	1
E_ε	Evaporation coefficient of obstacle pheromones	0.2
G_ε	Diffusion coefficient of obstacle pheromones	0.2
d_ε	Pheromone concentration produced by obstacles in one iteration	1
σ_0	Initial concentration of path pheromones	2
$\sigma_{\min}$	Minimum concentration of path pheromones	0.1
D_0	Range of influence	4
Q	Attenuation coefficient	1
λ_{Ta}	Weight of target pheromones	1
λ_{Th}	Weight of obstacle pheromones	−0.3
λ_{Tr}	Weight of path pheromones	0.3

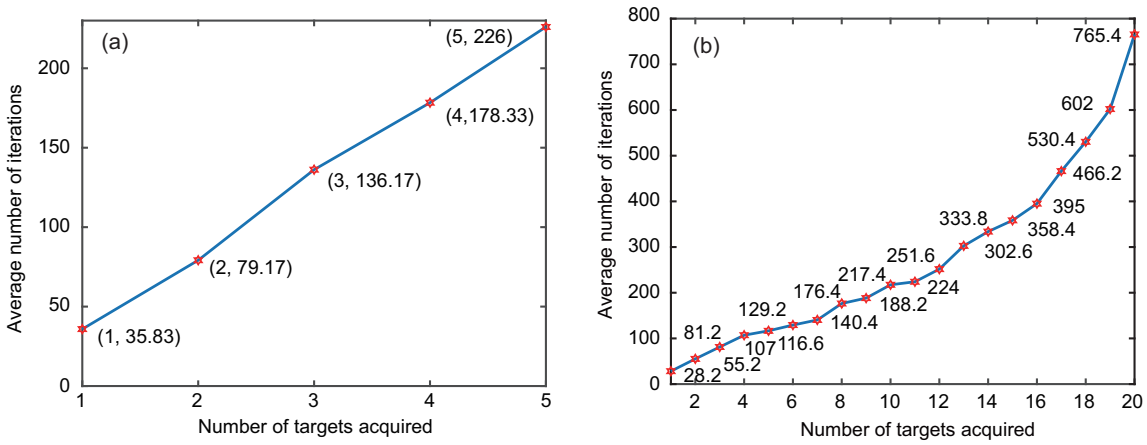

Fig. 4 Target acquisition rates of two maps of different sizes: (a) 50×50; (b) 100×100

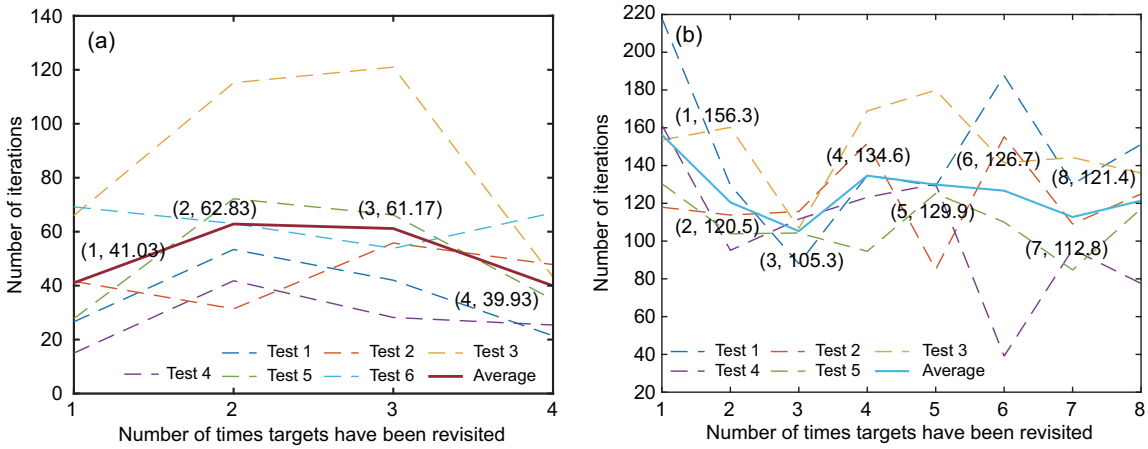

Fig. 5 Revisit response rates of two maps of different sizes: (a) 50×50; (b) 100×100

more steps because there are some unvisited areas in the map which appeal to the individuals to explore.

4.3.3 Global coverage

Global coverage means that the areas explored by the multiple UAVs in the sensor range account for the total areas. To highlight the advantages of the current algorithm more intuitively, we compare it with the exhaustive search algorithm which needs fixed routes. The results are displayed in Fig. 6. Obviously, compared with the linear growth of the exhaustive search algorithm, the proposed algorithm based on artificial pheromone potential field presents wider coverage and lower repetition rate. The reason that the coverage rate does not reach one is that there are unreachable obstacles. In addition, the exhaustive search algorithm with a fixed path is not robust or flexible, facing unexpected faults which cause a rapid decrease in the efficiency of the whole system. However, our algorithm with no fixed path can adapt dynamically to emergencies with strong robustness and fitness.

4.3.4 Analysis of path and pheromone deposit

To make the simulation results more intuitive and readable, the individual routes in the search process are shown in Fig. 7a. At the 185^{th} step, it is the first time that all targets in the map are found by the multi-UAV system. Fig. 7b is the path pheromone map at this step well matched with individuals' routes. It verifies the effectiveness of the pheromone mechanism. We analyze the target and obstacle pheromone deposit mechanism by sampling pheromone concentration during the iteration. The result in Fig. 7c is the target pheromone map at the 670^{th} step when three targets send a revisit signal and deposit pheromones. As shown in Fig. 7d, a synthesized pheromone map is calculated by Eq. (9), without considering the physical costs.

5 Navigation algorithm via flocking and stigmergy

The previous algorithm pays attention to designing individual's decision-making scheme and pheromone update strategy to address target detection and revisit scenarios. We have to consider that one target may require more than one agent to visit while some agents have limitations in perception and communication. To fulfill this demand, we put forward the navigation algorithm via flocking and stigmergy in this section. Note that we adjust the conventional individual decision scheme by replacing a pheromone scalar by a pheromone vector (Tang et al., 2019).

As depicted in Olfati-Saber (2006) and Su et al. (2009), the essence of Olfati-Saber's algorithm is based on a flocking model from nature, which is the classical algorithm in the field of multi-agent system control. Based on this classical setting, we divide the swarm into leaders and followers. An artificial pheromone potential field is used to guide the leaders who have relatively strong communication and perception skills. Followers are controlled by Olfati-Saber's flocking algorithm.

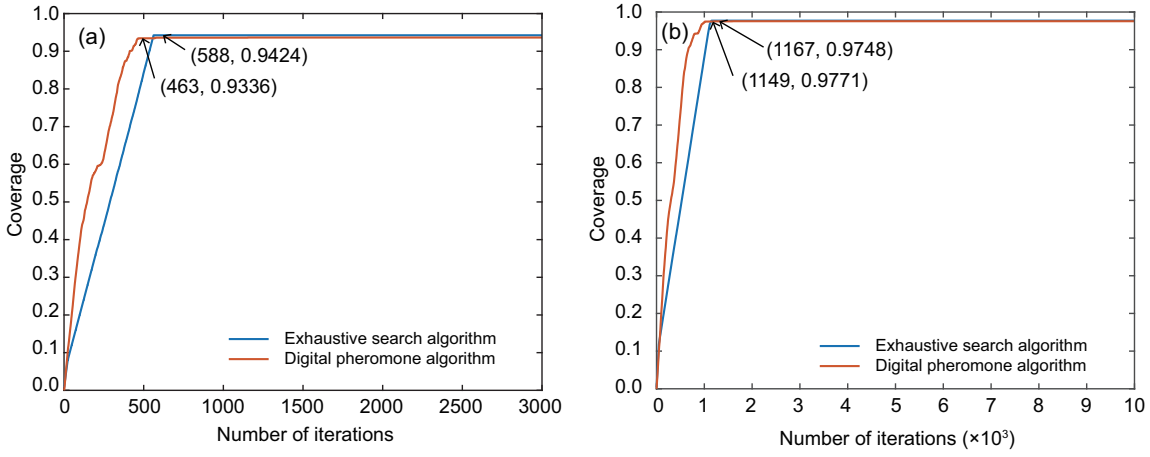

Fig. 6 Global coverage of two maps of different sizes: (a) 50 × 50; (b) 100 × 100

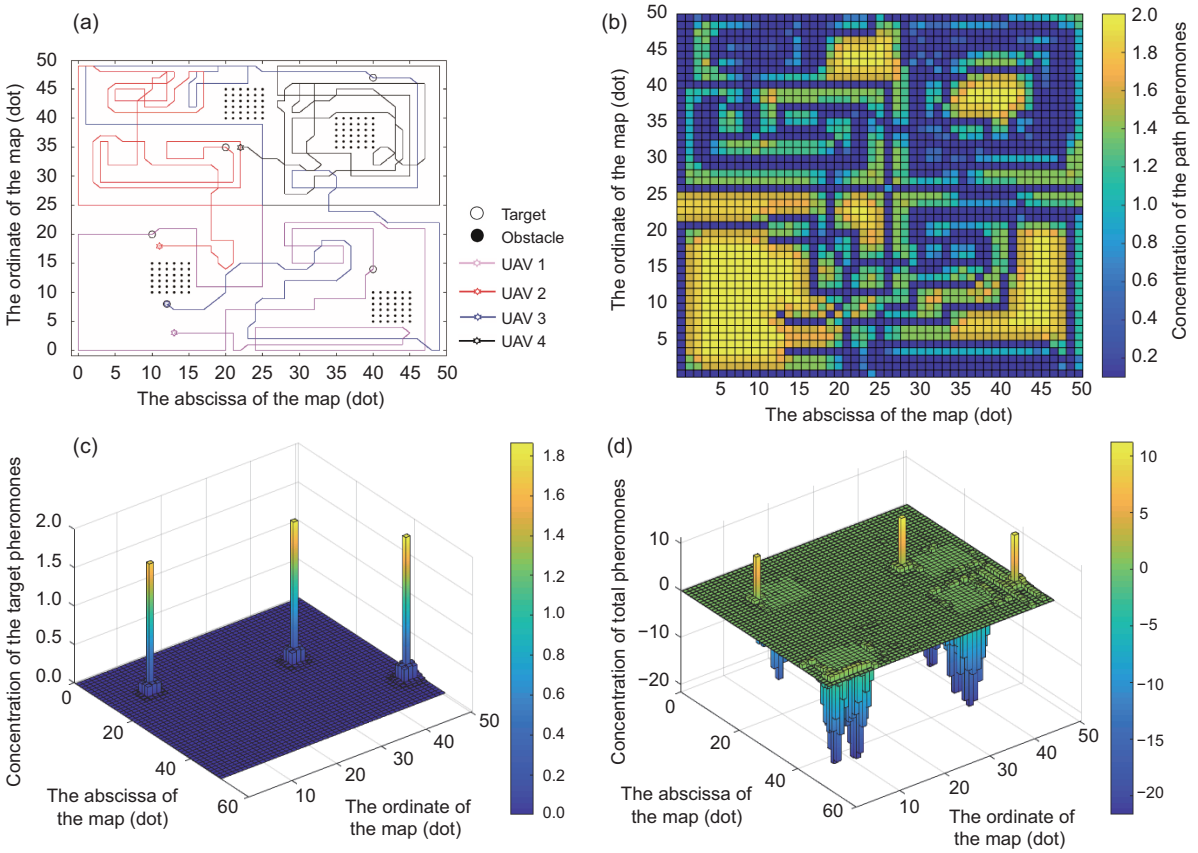

Fig. 7 Analysis of path and pheromones deposit for the 50×50 map: (a) the path at the 185^{th} iteration when all targets have been detected for the first time; (b) distribution of path pheromones at the 185^{th} iteration; (c) distribution of target pheromones at the 670^{th} iteration when some targets need to be revisited; (d) the total pheromone map combining three pheromones by weight

5.1 Algorithm

The decision-making algorithm is divided into two parts, i.e., the leader part and the follower part.

5.1.1 Leader

The circle of the leader's sensor range is divided into eight sectors (Fig. 8). Let $S = \{1, 2, \ldots, 8\}$ represent the set of sectors and d is an element of S, $d \in S$. Denote by $\boldsymbol{\tau}_{ij}^t$ the vector pheromones for the i^{th} point to the j^{th} point at the t^{th} iteration, which is calculated by

$$\boldsymbol{\tau}_{ij}^t = \frac{\tau(i,t) - \tau(j,t)}{\|\boldsymbol{q}_i^{\text{L}} - \boldsymbol{q}_j\|} \cdot \frac{\boldsymbol{q}_i^{\text{L}} - \boldsymbol{q}_j}{\|\boldsymbol{q}_i^{\text{L}} - \boldsymbol{q}_j\|}, \tag{12}$$

where $\|\cdot\|$ represents the Euclidean norm, $\tau(i,t)$ is the density of pheromones in the i^{th} point at the t^{th} step as defined in Eq. (1), $\boldsymbol{q}_i^{\text{L}}$ is the current position of the leader, and $\boldsymbol{q}_j$ is the coordinate of the j^{th} point. Thus, $\dfrac{\tau(i,t) - \tau(j,t)}{\|\boldsymbol{q}_i^{\text{L}} - \boldsymbol{q}_j\|}$ is a scalar coefficient to be equivalent to the norm of $\boldsymbol{\tau}_{ij}^t$. Denote by $\boldsymbol{\tau}_d^t$ the sum of $\boldsymbol{\tau}_{ij}^t$ in the same sector, calculated by

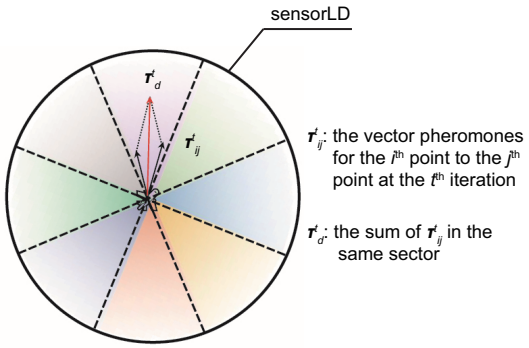

Fig. 8 Vector pheromones schematic

$$\boldsymbol{\tau}_d^t = \sum_{j \in J(d)} \boldsymbol{\tau}_{ij}^t, \tag{13}$$

where $J(d)$ is the point set within the d^{th} sector. The calculations of the other two kinds of pheromones, $\boldsymbol{\varepsilon}_d^t$ and $\boldsymbol{\sigma}_d^t$, are defined similar to the target pheromones, and thus are omitted here to avoid repetition. Denote by $\boldsymbol{s}_d^t$ the weighted sum of the three different semantic pheromones:

$$\boldsymbol{s}_d^t = \lambda_{\text{Ta}}\boldsymbol{\tau}_d^t + \lambda_{\text{Th}}\boldsymbol{\varepsilon}_d^t + \lambda_{\text{Tr}}\boldsymbol{\sigma}_d^t. \tag{14}$$

Let $\boldsymbol{s}^t = \max_d \|\boldsymbol{s}_d^t\|$, where $d \in S$ is selected as a reference to the direction of velocity to calculate the velocity and position of the next step. Denote by ρ a coefficient between $\boldsymbol{s}^t$ and $\boldsymbol{v}_{t+1}^L$ which decides the value of the velocity.

$$\boldsymbol{v}_{t+1}^{\text{L}} = \rho \cdot \frac{\boldsymbol{s}^t}{\|\boldsymbol{s}^t\|}, \tag{15}$$

$$\boldsymbol{q}_{t+1}^{\text{L}} = \boldsymbol{q}_t^{\text{L}} + \boldsymbol{v}_{t+1}^{\text{L}}. \tag{16}$$

The integrated decision-making algorithm of the leader is shown in Algorithm 2.

Algorithm 2 Decision-making algorithm of the leader

Input: local pheromone map of the current position; current location vector, $\boldsymbol{q}_t^{\text{L}}$; current velocity vector, $\boldsymbol{v}_t^{\text{L}}$

Output: location vector after updating, $\boldsymbol{q}_{t+1}^{\text{L}}$; velocity vector after updating, $\boldsymbol{v}_{t+1}^{\text{L}}$

1: **if** having the center of the target region in sensorLD **then**
2: Go there
3: End the mission as a leader
4: Become a follower
5: **end if**
6: Divide the sensor range into eight sectors $d \in S$, $S = \{1, 2, \ldots, 8\}$ (Fig. 8)
7: Compute the total pheromone vectors $\boldsymbol{\tau}_d^t$, $\boldsymbol{\varepsilon}_d^t$, and $\boldsymbol{\sigma}_d^t$
8: Compute the weighted sum of different semantic pheromones, $\boldsymbol{s}_d^t$
9: Compute $\boldsymbol{v}_{t+1}^{\text{L}}$
10: Compute $\boldsymbol{q}_{t+1}^{\text{L}} = \boldsymbol{q}_t^{\text{L}} + \boldsymbol{v}_{t+1}^{\text{L}}$
11: **return** $\boldsymbol{q}_{t+1}^{\text{L}}$ and $\boldsymbol{v}_{t+1}^{\text{L}}$

5.1.2 Follower

A simplified version of Olfati-Saber's flocking algorithm is used in this subsection to match the scenario. A leader is designed to replace the virtual leader. When one of the followers makes a moving decision, the states of the leader and other followers need to be used as a reference. To distinguish among different clusters and consider some constraint conditions, $N_k(t)$ is used to represent the followers within the sensor range of the k^{th} follower:

$$N_k(t) = \{j : \|\boldsymbol{q}_t^k - \boldsymbol{q}_t^j\| < r, j = 1, 2, \ldots, N, j \neq k\}. \tag{17}$$

To construct a smooth collective potential of a flock and spatial adjacency matrix of a proximity net (Olfati-Saber, 2006), a non-negative map called σ-norm is defined:

$$\|\boldsymbol{z}\|_\sigma = \frac{1}{\varepsilon}\left(\sqrt{1+\varepsilon\|\boldsymbol{z}\|^2} - 1\right), \tag{18}$$

where $\varepsilon \in (0, 1)$ is a fixed parameter and in this study we set $\varepsilon = 0.1$. The modified Olfati-Saber's flocking algorithm is given by

$$\begin{aligned}\boldsymbol{v}_{t+1}^k = &\sum_{j\in N_k(t)} \varphi_\alpha\left(\|\boldsymbol{q}_t^j - \boldsymbol{q}_t^k\|_\sigma\right)\boldsymbol{n}_{kj} \\ &+ \sum_{j\in N_k(t)} a_{kj}(t)(\boldsymbol{v}_t^j - \boldsymbol{v}_t^k) \\ &- c_1(\boldsymbol{q}_t^k - \boldsymbol{q}_t^{\text{L}}) - c_2(\boldsymbol{v}_t^k - \boldsymbol{v}_t^{\text{L}}).\end{aligned} \tag{19}$$

We sum over the variations whose indices are in $N_k(t)$. c_1 and c_2 represent the weights of the leader's influence on the follower's acceleration, and we set $c_1 = 0.6$ and $c_2 = 0.4$ empirically. $\boldsymbol{v}_{t+1}^k$ is the velocity vector after updating, decided by the leader and followers in the sensor range. We choose an inverse function of smooth descent to define $\varphi_\alpha(z)$:

$$\varphi_\alpha(z) = \frac{1}{z}. \tag{20}$$

Denote by $\boldsymbol{n}_{kj}$ the unit vector from the j^{th} agent to the k^{th} agent:

$$\boldsymbol{n}_{kj} = \frac{\boldsymbol{q}_t^j - \boldsymbol{q}_t^k}{\sqrt{1+\varepsilon\|\boldsymbol{q}_t^k - \boldsymbol{q}_t^j\|_\sigma^2}}. \tag{21}$$

Define $a_{kj}(t)$ as

$$a_{kj}(t) = \begin{cases} 0, & j = k, \\ \rho_h\dfrac{\|\boldsymbol{q}_t^k - \boldsymbol{q}_t^j\|_\sigma}{r}, & j \neq k, \end{cases} \tag{22}$$

where

$$\rho_h(z) = \begin{cases} 1, & z \in [0, h), \\ \dfrac{1}{2}\left[1 + \cos\left(\pi\dfrac{z-h}{1-h}\right)\right], & z \in [h, 1), \\ 0, & \text{otherwise}, \end{cases} \tag{23}$$

where $h \in (0,1)$ and we choose $h = 0.5$ here empirically. Finally, we can compute the location vector after updating by

$$\boldsymbol{q}_{t+1}^k = \boldsymbol{q}_t^k + \boldsymbol{v}_{t+1}^k. \tag{24}$$

The integrated decision-making algorithm of the followers is shown in Algorithm 3.

Algorithm 3 Decision-making algorithm of followers

Input: local pheromone map of the current position; current location vector of the leader and followers, $\boldsymbol{q}_t^{\mathrm{L}}$, $\boldsymbol{q}_t^k$; current velocity vector of the leader and followers, $\boldsymbol{v}_t^{\mathrm{L}}$, $\boldsymbol{v}_t^k$

Output: location vector after updating, $\boldsymbol{q}_{t+1}^k$; velocity vector after updating, $\boldsymbol{v}_{t+1}^k$

1: **if** the leader has reached the center of the target region **then**
2: Execute the target detection algorithm based on digital pheromones
3: **else**
4: Obtain the states of the leader and the other followers
5: Compute $\boldsymbol{q}_{t+1}^k$ and $\boldsymbol{v}_{t+1}^k$ based on Eqs. (17)–(24) // execute the flocking algorithm
6: **end if**
7: **return** $\boldsymbol{q}_{t+1}^k$ and $\boldsymbol{v}_{t+1}^k$

5.2 Simulation and results

To verify the availability of the navigation algorithm, we design the simulation according to the scenario model and computation function in the previous sections. Several pivotal parameters are listed in Table 2. To make the results readable, we plot the path diagram in Fig. 9. It is at the 67$^{\mathrm{th}}$ step that the leader reaches the center of the target region. The leader, guided by the artificial pheromone potential field, uses vector pheromones to find the center of the target region in finite iterations efficiently in line with the forecast.

To show the superiority of the vector, we compare the results with those guided by vector pheromones with scalar pheromones. The results are given in Fig. 10. It is obvious that vector pheromones which only use 67 iterations to reach the center perform better than the scalar one which needs 102 iterations.

Table 2 Simulation parameters of the navigation algorithm

Parameter	Description	Value
N_{c}	Number of total iteration steps	500
sensorLD	Sensor radius of the leader	5
λ_{Ta}	Weight of target pheromones	1
λ_{Th}	Weight of obstacle pheromones	−0.3
λ_{Tr}	Weight of path pheromones	0.3
ρ	Coefficient of the velocity	2
h	Parameters of Olfati-Saber's algorithm	0.5
ε		0.1
c_1		0.6
c_2		0.4

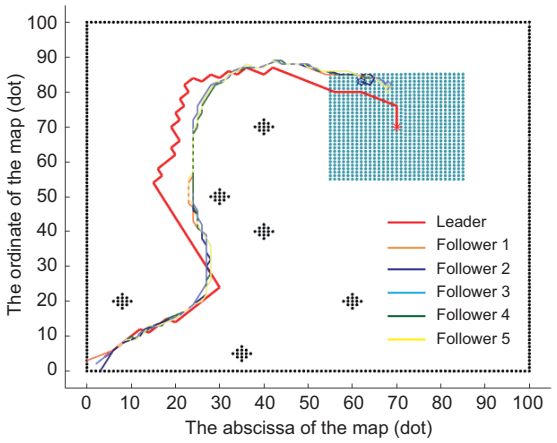

Fig. 9 The path at the 67$^{\mathrm{th}}$ iteration when the leader reaches the center of the target region. References to color refer to the online version of this figure

6 Conclusions and future work

In this study we explore mainly the application of digital pheromones in multi-UAV system control. Taking into account the development of multi-UAV systems, combined with the current mainstream unmanned system controlling algorithms, we have designed an algorithm for target detection and revisit in environments with limited prior knowledge. We have also used Olfati-Saber's flocking algorithm to help solve the limitations of sensor range and communication. Major contributions are summarized as follows: (1) Based on three primary characteristics of digital pheromones, we have optimized the updating mechanism and fusion scheme of different semantic pheromones; (2) We have designed the decision-making algorithm by expanding the reference range to make more accurate decisions; (3) We have used vector pheromones instead of scalar pheromones for a more efficient decision-making procedure; (4) We

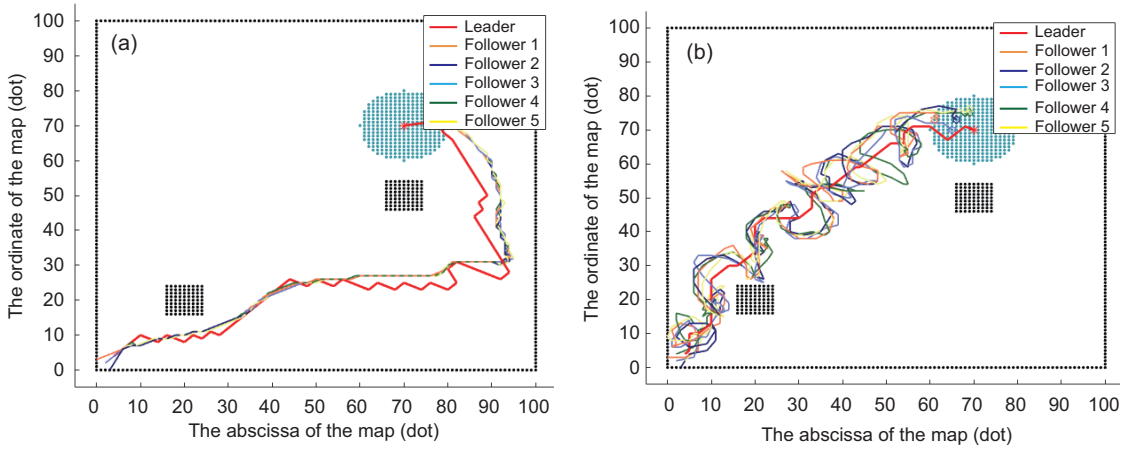

Fig. 10 Performances of vector pheromones (a) and scalar pheromones (b). (a) shows the path at the 67th iteration when the leader reaches the center of the target region and (b) shows the path at the 102nd iteration when the leader reaches the center of the target region. References to color refer to the online version of this figure

have modified Olfati-Saber's flocking algorithm to better fit unknown environments with the limitations of sensor range and communication; (5) We have verified the effectiveness of the aforementioned algorithm through extensive simulations.

To sum up, this work is meaningful in the domain of multi-agent system control and there is much further work to be done, so as to optimize the digital pheromone mechanism based on stigmergy and explore better control algorithms. Future work will focus on testing the performance of the algorithm in robot entities like KHEPERAIV (Soares et al., 2015), using evolution algorithms such as differential and genetic evolution (Cimino et al., 2019) for parameter optimization.

Contributors

Yan SHAO conducted most of research simulations and analyses, while Zhi-feng ZHAO pointed out the key research directions. Yan SHAO drafted the manuscript. Rong-peng LI helped organize the manuscript. Yan SHAO, Zhi-feng ZHAO, Rong-peng LI, and Yu-geng ZHOU revised and finalized the paper.

Compliance with ethics guidelines

Yan SHAO, Zhi-feng ZHAO, Rong-peng LI, and Yu-geng ZHOU declare that they have no conflict of interest.

References

Alfeo AL, Cimino MGCA, de Francesco N, et al., 2018a. Design and simulation of the emergent behavior of small drones swarming for distributed target localization. *J Comput Sci*, 29:19-33. https://doi.org/10.1016/j.jocs.2018.09.014

Alfeo AL, Cimino MGCA, Egidi S, et al., 2018b. A stigmergy-based analysis of city hotspots to discover trends and anomalies in urban transportation usage. *IEEE Trans Intell Transp Syst*, 19(7):2258-2267. https://doi.org/10.1109/TITS.2018.2817558

Alfeo AL, Cimino MGCA, de Francesco N, et al., 2018c. Swarm coordination of mini-UAVs for target search using imperfect sensors. *Intell Dec Technol*, 12(2):149-162. https://doi.org/10.3233/IDT-170317

Ando Y, Fukazawa Y, Masutani O, et al., 2006. Performance of pheromone model for predicting traffic congestion. Proc 5th Int Joint Conf on Autonomous Agents and Multiagent Systems, p.73-80. https://doi.org/10.1145/1160633.1160642

Cimino MGCA, Lega M, Monaco M, et al., 2019. Adaptive exploration of a UAVs swarm for distributed targets detection and tracking. Proc 8th Int Conf on Pattern Recognition Applications and Methods, p.1-8.

Dai AN, Zhao ZF, Li RP, et al., 2020. Evaluation mechanism of collective intelligence for heterogeneous agents group. *IEEE Access*, 8:28385-28394. https://doi.org/10.1109/ACCESS.2020.2971278

Dorigo M, di Caro G, Gambardella LM, 1999. Ant algorithms for discrete optimization. *Artif Life*, 5(2):137-172. https://doi.org/10.1162/106454699568728

Eberhart R, Kennedy J, 1995. A new optimizer using particle swarm theory. Proc 6th Int Symp on Micro Machine and Human Science, p.39-43. https://doi.org/10.1109/MHS.1995.494215

Karaboga D, 2005. An Idea Based on Honey Bee Swarm for Numerical Optimization. Technical Report-tr06, Erciyes University, Turkey.

Kennedy J, Eberhart R, 1995. Particle swarm optimization. Proc Int Conf on Neural Networks, p.1942-1948.

Kuyucu T, Tanev I, Shimohara K, 2015. Superadditive effect of multi-robot coordination in the exploration of

unknown environments via stigmergy. *Neurocomputing*, 148:83-90.
https://doi.org/10.1016/j.neucom.2012.07.062

Liu Z, Gao XG, Fu XW, 2018. A cooperative search and coverage algorithm with controllable revisit and connectivity maintenance for multiple unmanned aerial vehicles. *Sensors*, 18(5):1472.
https://doi.org/10.3390/s18051472

Micieta B, Edl M, Krajcovic M, et al., 2018. Delegate mass for coordination and control of one-directional AGV systems: a proof-of-concept. *Int J Adv Manuf Technol*, 94(1-4):415-431.
https://doi.org/10.1007/s00170-017-0915-8

Olfati-Saber R, 2006. Flocking for multi-agent dynamic systems: algorithms and theory. *IEEE Trans Autom Contr*, 51(3):401-420.
https://doi.org/10.1109/TAC.2005.864190

Reynolds CW, 1987. Flocks, herds, and schools: a distributed behavioral model. *ACM SIGGRAPH Comput Graph*, 21(4):25-34. https://doi.org/10.1145/37402.37406

Sauter JA, Matthews R, van Dyke Parunak H, et al., 2005. Performance of digital pheromones for swarming vehicle control. Proc 4th Int Joint Conf on Autonomous Agents and Multiagent Systems, p.903-910.
https://doi.org/10.1145/1082473.1082610

Senanayake M, Senthooran I, Barca JC, et al., 2016. Search and tracking algorithms for swarms of robots: a survey. *Robot Auton Syst*, 75:422-434.
https://doi.org/10.1016/j.robot.2015.08.010

Soares JM, Navarro I, Martinoli A, 2015. The Khepera IV mobile robot: performance evaluation, sensory data and software toolbox. Proc 2nd Iberian Robotics Conf, p.767-781.
https://doi.org/10.1007/978-3-319-27146-0_59

Soria E, Schiano F, Floreano D, 2019. The influence of limited visual sensing on the Reynolds flocking algorithm. Proc 3rd Int Conf on Robotic Computing, p.138-145.
https://doi.org/10.1109/IRC.2019.00028

Su HS, Wang XF, Lin ZL, 2009. Flocking of multi-agents with a virtual leader. *IEEE Trans Autom Contr*, 54(2):293-307.
https://doi.org/10.1109/TAC.2008.2010897

Tang QR, Xu ZP, Yu FC, et al., 2019. Dynamic target searching and tracking with swarm robots based on stigmergy mechanism. *Robot Auton Syst*, 120:103251.
https://doi.org/10.1016/j.robot.2019.103251

van Dyke Parunak H, Brueckner S, Sauter J, 2002. Digital pheromone mechanisms for coordination of unmanned vehicles. Proc 1st Int Joint Conf on Autonomous Agents and Multiagent Systems, p.449-450.
https://doi.org/10.1145/544741.544843

Vásárhelyi G, Virágh C, Somorjai G, et al., 2018. Optimized flocking of autonomous drones in confined environments. *Sci Rob*, 3(20):eaat3536.
https://doi.org/10.1126/scirobotics.aat3536

Yang F, Ji XL, Yang CW, et al., 2017. Cooperative search of UAV swarm based on improved ant colony algorithm in uncertain environment. Proc IEEE Int Conf on Unmanned Systems, p.231-236.
https://doi.org/10.1109/ICUS.2017.8278346